- 1 Estimating Spatial and Temporal Patterns of Urban Building Anthropogenic Heat
- 2 using a bottom-up City Building Heat Emission Model
- 3 Wei Chen^a, Yuyu Zhou^{a,*}, Yanhua Xie^b, Gang Chen^c, Ke Jack Ding^a, Dan Li^d
- 4 a Department of Geological and Atmospheric Sciences, Iowa State University, Ames, IA 50011,
- 5 USA
- 6 b DOE Great Lakes Bioenergy Research Center, University of Wisconsin-Madison, Madison, WI
- 7 53726, USA
- 8 ^c Laboratory for Remote Sensing and Environmental Change (LRSEC), Department of Geography
- 9 and Earth Sciences, University of North Carolina at Charlotte, Charlotte, NC 28223, USA
- 10 d Department of Earth and Environment, Boston University, Boston, MA 02215, USA
- * Corresponding author
- 12 Email address: yuyuzhou@iastate.edu (Y. Zhou)

Abstract: Anthropogenic heat (AH) emission from buildings is a key contributor to the urban heat island (UHI) effect. Although an improved understanding of spatiotemporal patterns of building AH is highly needed for mitigating UHI effect, such information is still limited in high spatiotemporal resolution at the city level. In this study, a bottom-up city building heat emission model (CityBHEM) was developed to investigate temporal variations of building AH from three components (i.e., envelope convection, zone infiltration and exfiltration, and HVAC system) for all buildings in Boston, United States. First, buildings in Boston were grouped into eleven commercial and five residential building prototypes based on building type, construction year, and foundation type. Second, an end-use-based calibration was developed to calibrate CityBHEM using U.S. Energy Information Administration's survey data. Finally, AH from all buildings in the city under actual weather conditions was calculated using the calibrated CityBHEM model together with building types and sizes. Results indicate that total building AH density of Back Bay neighborhood reaches the maximum value of 526 kWh/m² in summer (56% of HVAC system and 44% of envelope convection) and the minimum value of 369 kWh/m² in winter (54% of HVAC system, 24% of envelope convection and 22% of zone infiltration and exfiltration). In contrast, total building AH density of suburban neighborhoods is lower than 30 kWh/m² in summer and 20 kWh/m² in winter. Given that key inputs are publicly available, CityBHEM is transferable to other U.S. cities, enabling us to explore practical building energy-saving strategies for mitigating AH.

Keywords: Anthropogenic heat; Building heat emissions; Building energy model; Spatiotemporal

13

14

15

16

17

18

19

20

21

22

23

24

25

26

27

28

29

30

31

2

1. Introduction

32

33

34

35

36

37

38

39

40

41

42

43

44

45

46

47

48

49

50

51

52

53

54

Anthropogenic heat (AH) plays an important role in urban surface energy balance and urban climate (Nie et al., 2014; Zhou et al., 2012). AH originates primarily from energy consumption of buildings (e.g., heating, ventilation, and air-conditioning (HVAC) system), industrial activities, fuel combustion of vehicular traffic, and human activities (Sailor, 2011). In particular, AH from building sector accounts for 50% to 65% of the total AH, depending on seasons (Luo et al., 2020). Sailor and Lu investigated spatiotemporal patterns of AH from three sectors in 12 large US cities, and the results showed that AH from building sector accounted for 60% of the total AH during winter months and 50% of the total AH in summer. Given the importance of AH from building sector, improving building energy use efficiency would be a potential way to significantly reduce AH (DOE, 2015), serving as a breakthrough point where government agencies and researchers can implement intervention practices towards total AH reduction in urban environments (Chrysoulakis and Grimmond, 2016). With the knowledge of building AH patterns at the city level, researchers can quantify its contribution to urban heat island (UHI) (Li et al., 2017), and estimate its impact on thermal comfort (Chrysoulakis and Grimmond, 2016) and air quality (Xie et al., 2016; Yu et al., 2014). Therefore, it facilitates smart city planning by developing diverse and customized strategies to mitigate UHI effect. Moreover, ongoing population growth and economic development lead to unprecedented urbanization (Zhou et al., 2018, 2014), which significant increases urban building AH. However, it is challenging to estimate building AH due to its high dependence on weather conditions and occupant behaviors (Luo et al., 2020).

A variety of methods have been proposed to estimate building AH at various scales. These methods can be categorized into the top-down inventory-based and bottom-up physically-based (Sailor, 2011). The top-down inventory-based approaches have been widely used from regional

(Lu et al., 2016) to global scales (Dong et al., 2017). Based on the assumption that heat discharges from buildings highly correlate with energy consumption, monthly to annual government-reported energy consumption data were used to estimate building AH in top-down methods (Liu et al., 2021). However, such methods rely on the availability of energy consumption-related variables, e.g., cooling and heating degree days (Sailor et al., 2015), population density (Lindberg et al., 2013), local climate zones [10], and nighttime night radiance (Chen et al., 2019). As a result, the estimated building AH using top-down methods typically has coarse spatial resolution and limited temporal frequencies, which limits our understanding of spatiotemporal patterns of building AH at the city level. In addition, significantly differences between building AH and energy consumption has been found (Dhakal et al., 2004, 2003; Hong et al., 2019). To better capture building AH at finer spatial and temp scales, the bottom-up physically-based approach has been developed (Sailor, 2011) to calculate building AH and energy consumption separately, such as urban canopy meteorological models (e.g., the Building Effect Parameterization coupled with Building Energy Model (BEP + BEM) in Weather Research Forecasting (WRF) (Chow et al., 2014) and the town energy budget model (Masson, 2000)) and building energy models (e.g., EnergyPlus, eQuest, and DOE-2).

55

56

57

58

59

60

61

62

63

64

65

66

67

68

69

70

71

72

73

74

75

76

77

Urban canopy meteorological models are simplified building energy models (Takane et al., 2017). Buildings in urban canopy meteorological models are treated as simplified envelope structures containing physical attributes related to air conditioning system, thermal properties, and internal loads (e.g., occupants, lights, and appliances). Heat emissions from air conditioning consumption are estimated by solving an energy conservation equation (Chow et al., 2014). However, different occupant behaviors, thermal properties, and HVAC equipment types and efficiencies for different building types are not considered in these models even though they have

significant impact on spatiotemporal patterns of building AH (Hong et al., 2020). Compared to simplified envelope structures in urban canopy meteorological models, building energy models simulate AH more realistically with more detailed descriptions about construction materials, thermal zones, HVAC systems, occupancy characteristics, and operation schedules for different commercial and residential building prototypes (Crawley et al., 2001). Integrating these building energy models with GIS databases containing building types and sizes allows us to investigate spatiotemporal patterns of building AH at the city level with consideration of building types. For example, Hisieh *et al.* (Hsieh et al., 2007) used EnergyPlus and a total of 10 building prototypes (4 residential and 6 commercial) to interpret spatiotemporal patterns of AH discharged from HVAC system on a summer day in Taipei, Taiwan. Sailor *et al.* (Sailor et al., 2007) conducted a similar study in Houston, USA using eQuest and a total of 13 building prototypes (2 residential and 11 commercial).

However, existing city-wide building AH estimation and analyses mainly focus on total building AH (Dhakal et al., 2004, 2003; Luo et al., 2020) or AH from HVAC system (Hsieh et al., 2007; Sailor et al., 2007). Except for HVAC system, AH also occurs as convective heat due to temperature difference between exterior surface of buildings and outdoor air as well as heat released from infiltration (e.g., exhaust fans in kitchens, bathrooms, and laundry rooms) and exfiltration (e.g., opening windows and doors and unintended airflow through cracks) (Chrysoulakis and Grimmond, 2016; Hong et al., 2020). Hong *et al.* (Hong et al., 2020) estimated building AH from these three components, i.e., envelope convection, zone infiltration and exfiltration, and HVAC system, in four weather conditions for 16 buildings prototypes (15 commercial and one residential). Ferrando *et al.* (Ferrando et al., 2021) evaluated the impact of energy-saving strategies on these three AH components in three weather conditions for 2

residential building prototypes to improve the understanding of the relationship between heat emission and the corresponding strategies. Compared to the total AH, an improved understanding of its components is of great help for policymakers in developing strategies tailored to a specific city or region.

While previous studies showed promising results on estimating building AH, an improved understanding of building AH from various components resolved at high spatial and temporal resoultions at the city level is still highly needed. In this study, we aimed to address this challenge by developing a bottom-up city building heat emission model (CityBHEM) to investigate spatiotemporal patterns of building AH from all components in Boston, U.S. The model was built upon the first and popular building energy model EnergyPlus version 9.4, where we capitalized on its ability to directly integrating the calculation of energy consumption with the quantification of AH. The remainder of this paper describes the study area and data (Section 2), the selection of building prototypes (Section 3.1) the end-use-based calibration (Section 3.2), the building AH estimation (Section 3.3), results (Section 4), discussion (Section 5), and concluding remarks (Section 6).

2. Study area and data

The study area is Boston, the largest city in Massachusetts, located in American Society of Heating, Refrigerating and Air-Conditioning Engineers (ASHRAE) Climate Zone 5A with warm, humid summers and cold, stormy winters (Melaas et al., 2016). As one of the most populous metropolitans in the U.S., Boston has about 4.5 million inhabitants in 2018 (Chang et al., 2021). In terms of urban morphology, there are skyscrapers in downtown Boston and low-lying residential areas in suburbs (Figure 1). Due to its dense population and complex urban morphology, observational studies indicated strong UHI effects in Boston (Wang et al., 2017).

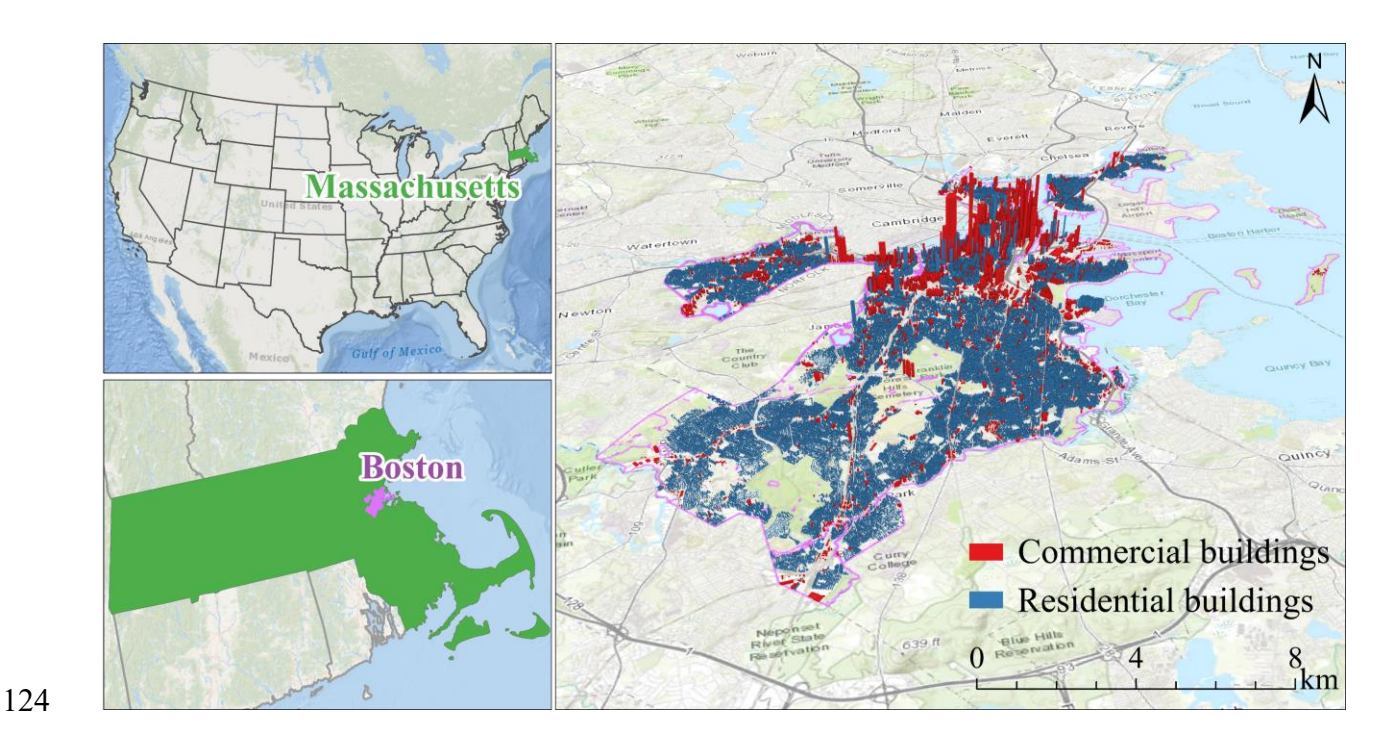


Figure 1. Study area of Boston, U.S. with 3D building information.

The key data used in this study include building prototypes, building footprints, assessor's parcels, and building energy consumption survey data (Table 1). Building footprints and assessor's parcels in circa 2017 were obtained from Boston government online data portal. While the footprint data shows building location and shape, the assessor's parcel data provides detailed information on building types, construction year, and the number of floors. Sixteen building prototypes (fifteen commercial and one residential) with three construction year categories [existing buildings constructed before 1980 ("pre-1980"), existing buildings constructed in or after 1980 ("post-1980"), and new construction ("new-2004")] were developed by the U.S. Department of Energy (DOE). Four residential building prototypes with four foundation types (i.e., slab, crawlspace, heated basement, and unheated basement) and five versions (i.e., 2006, 2009, 2012, 2015, 2018) of the International Energy Conservation Code (IECC) were developed by the Pacific Northwest National Laboratory (PNNL). Building energy consumption surveys were obtained from U.S. Energy Information Administration (EIA), including the Residential Energy

Consumption Survey (RECS) dataset from 2009 and the Commercial Building Energy
Consumption Survey (CBECS) from 2012.

Table 1. Summary of data sources in this study.

Data	Source	Year
Commercial building prototypes	https://www.energy.gov/eere/buildings/comm ercial-reference-buildings	N/A
Residential building prototypes	https://www.energycodes.gov/development/re sidential/iecc_models	N/A
Building footprints	https://data.boston.gov/	2017
Assessor's parcels	https://data.boston.gov/	2017
Commercial building energy consumption survey	https://www.eia.gov/consumption/commercial	2012
Residential building energy consumption survey	https://www.eia.gov/consumption/residential	2009

3. Methodology

In this study, a CityBHEM framework was built to estimate building AH and its three components (Figure 2). First, building prototypes were proposed to represent residential and commercial buildings in the study area. Second, an end-use-based calibration method of building energy consumptions was developed for all building prototypes. Finally, hourly building AH and

its three components for all buildings in the study area were calculated using AH intensities from the calibrated prototypes together with footprint areas and number of floors. More details about each step are presented in the following sections.

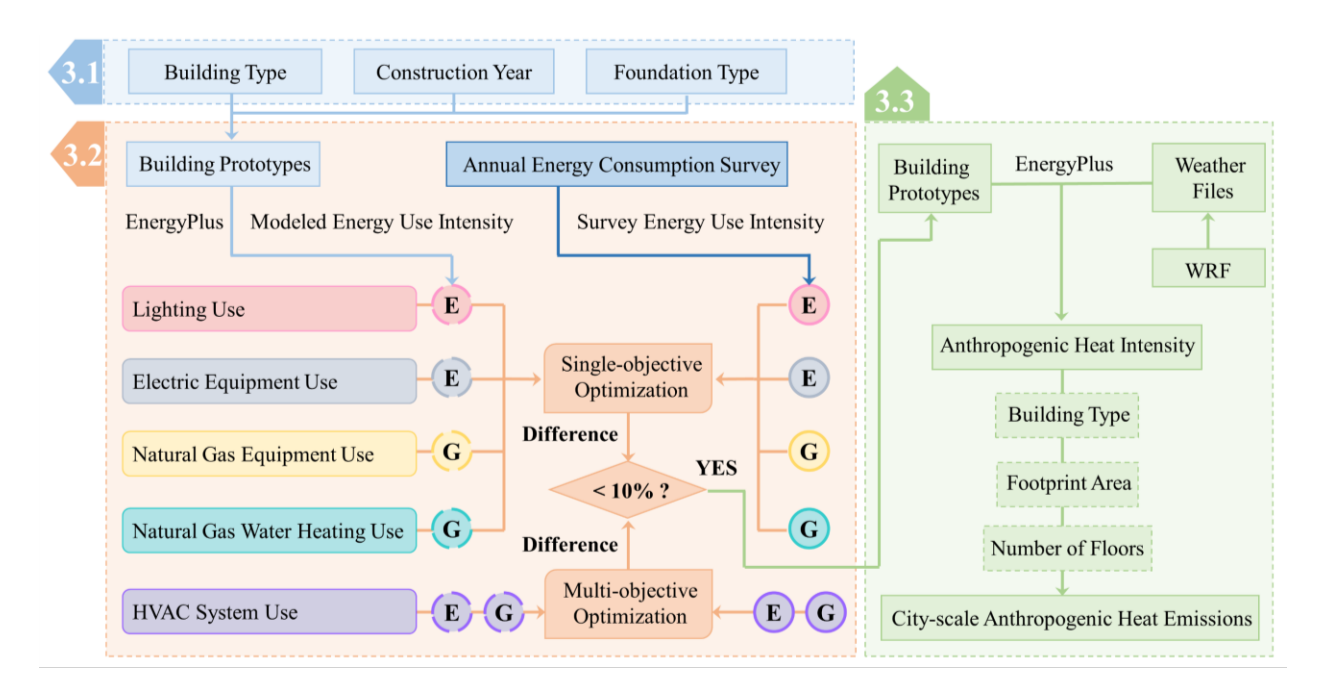


Figure 2. The proposed CityBHEM. E represents electricity and G represents natural gas.

3.1 Selection of building prototypes

Building prototypes were determined based on realistic building characteristics in Boston including building types, construction years, and foundation types. After assessing total floor area of each construction year category and each commercial building type, the "pre-1980" of DOE building prototypes and the 2006 IECC version of PNNL building prototypes were used (Figure 3A). Building types (i.e., primary school, outpatient health care, small hotel, and quick-service restaurant) that account for a small proportion of total floor area were grouped into their similar building types (i.e., secondary school, hospital, large hotel, and full-service restaurant) (Figure 3B). After assessing the total floor area of each residential foundation type in RECS Massachusetts census region (Figure 3C), PNNL residential building prototypes with an unheated basement were

used. In summary, 11 commercial building prototypes, including full-service restaurant (Restaurant), hospital, large hotel (Hotel), large office, medium office, small office, secondary school (School), stand-alone retail (Retail), strip mall, supermarket, and warehouse, and 5 residential building prototypes including midrise apartment (Midrise MF), single-family electricity resistance unheated basement (SF-electricity), single-family gas furnace unheated basement (SF-gas), multi-family electricity resistance unheated basement (MF-electricity), and multi-family gas furnace unheated basement (MF-gas) were used in this study.

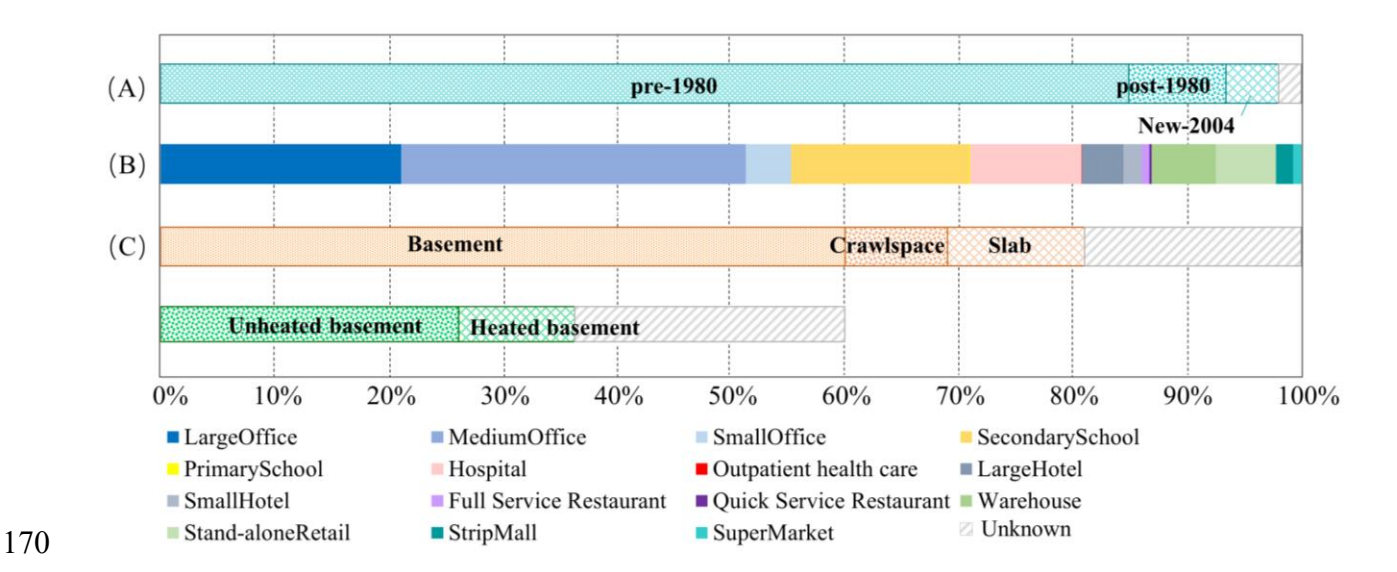


Figure 3. Building floor area in Boston by construction year (A) and commercial types (B), and buildings in RECS Massachusetts census region by foundation types (C).

3.2 End-use-based calibration

An end-use-based calibration method was developed to minimize the difference (%) between energy use intensities (EUIs) from building prototypes and building energy consumption surveys (hereinafter referred to as "modeled-survey EUIs"). This method utilized an automatic optimization algorithm, Non-dominated Sorting Genetic Algorithm (NSGA-II) (Li et al., 2018), to minimize modeled-survey EUIs iteratively for each end-use (i.e., HVAC system, water heating,

lighting, and equipment) by adjusting each related parameter within lower and upper bounds. First, survey EUIs were calculated for electric and natural gas consumption by end-uses as reference values of calibration. Second, to-be-tuned parameters in building prototypes were selected and then categorized by their impact on end-uses. Third, the automatic calibration process was conducted for each end-use to achieve an optimal value for each parameter. Finally, these optimal values of parameters were used to update building prototypes.

3.2.1 Reference data

Survey EUIs from energy consumption surveys in the census regions where Boston locates were used as reference data to calibrate building prototypes. Regional mean EUIs of electric and natural gas consumption by end-uses from the northeast census region in CBECS and the Massachusetts census region in RECS for each type of building were calculated, respectively. Because of the inconsistency of end-use categories in EnergyPlus and survey data, a lookup table of end-use categories between these two data (Table 2) was built.

Table 2. Lookup table of end-use categories between EnergyPlus and survey data.

Categories in	HVAC system	Lighting	Equipment	Water heating
this study				
Categories in	Heating use, Cooling	Lighting use	Refrigeration use, Cooking	Water heating
CBECS	use, Ventilation use		use, Office equipment use,	
			Computing use,	
			Miscellaneous use	
Categories in	Space Heating, Air-	Other purposes (appliances, electronics, lighting,		Water heating
RECS	conditioning	and miscellaneous uses), Refrigeration		

Categories in	Heating use, Cooling	Interior lighting,	Interior equipment, Exterior	Water heating
EnergyPlus	use, Fan, Pump, Heat	Exterior lighting	equipment	
	rejection, Heat recovery			

3.2.2 To-be-tuned parameters

193

194

195

196

197

198

199

200

201

202

203

204

205

206

207

208

209

To-be-tuned parameters, which have important impacts on the calibration process, were determined through an input-output sensitivity analysis using EnergyPlus for each end-use (O'Neill et al., 2011). By changing values of different input parameters related to an end-use at an interval of 0.1, parameters with the largest output changes in the corresponding end-use were selected as to-be-tuned parameters for this end-use category (Table 3). The upper and lower bounds of to-be-tuned parameters were determined based on ASHRAE Standards and other versions of building prototypes. Power density of lighting and equipment as well as occupancy density were tuned using an upper and lower bound of $\pm 50\%$ from original values (Chen et al., 2020; Qiu et al., 2018). Their diurnal schedules, varying between 0 (fully off) and 1 (fully on), were scaled up or down $\pm 30\%$ of all schedule values so that the original diurnal pattern was retained (Sun et al., 2016). Cooling and heating setpoints of HVAC system were allowed to be tuned using an upper and lower bound calculated by Eq. (1) and Eq. (2) in ANSI/ASHRAE Standard 55 (ASHRAE Standards 55, 2017). Their diurnal schedules were adjusted by increasing or decreasing all setpoint values by a delta temperature (its range is listed in Table 3) (Sun et al., 2016). In particular, for residential building prototypes, effective leakage area was selected as an additional parameter to further minimize modeled-survey EUIs for HVAC use (Figure 4C).

Upper bound_{heating/cooling set point} =
$$0.31 \times \overline{t_{ma(out)winter/summer}} + 21.3$$
 (1)

Lower bound_{heating/cooling set point} =
$$0.31 \times \overline{t_{ma(out)winter/summer}} + 14.3$$
 (2)

where $\overline{t_{ma(out)winter/summer}}$ represents mean outdoor air temperature in wintertime (December, January, and February) and summertime (June, July, and August) of 2012. Air temperature data is from meteorological station observations at Boston Logan International Airport.

Table 3. List of to-be-tuned parameters in the calibration process.

215

End-use category	Parameter	Upper and lower bound
Lighting, equipment, and water heating	Power density	[-50%, +50%]
	Schedule	[-30%, +30%]
HVAC system	Occupancy density	[-50%, +50%] for commercial
	Window U-factor	[0.5, 1.987] for residential (ASHRAE Standards 90.2, 2007),[0.1, 3.24] for commercial (ASHRAE Standards 90.1, 1999)
	Window Solar heat gain coefficient	[0.1, 0.4] (ASHRAE Standards 90.1, 1999; ASHRAE Standards 90.2, 2007)
	Cooling/heating setpoint and its schedule	$[Lower bound_{cooling/heating \ set \ point} - \\ Max_{schedule \ values}, \\ Upper bound_{cooling/heating \ set \ point} - \\ Min_{schdule \ values}]$
	Effective leakage area	[-62.5%, +166%] for residential

3.2.3 Automatic calibration

216

217

218

Optimal values of to-be-tuned parameters were automatically determined using the NSGA-II algorithm with objective functions. This algorithm can modify values of to-be-tuned parameters within their corresponding upper and lower bounds (list in Table 3) iteratively to achieve the smallest modeled-survey EUIs by minimizing objective functions. Two objective functions were designed for electricity (Eq. (3)) and natural gas (Eq. (4)), respectively. During the calibration process of each building prototype, the NSGA-II algorithm with a single-objective function was separately applied in the calibration of lighting (Eq. (3)), electric equipment (Eq. (3)), natural gas equipment (Eq. (4)), and natural gas water heating uses (Eq. (4)). HVAC electric and natural gas uses were simultaneously calibrated using the NSGA-II algorithm with multi-objective functions (Eq. (3) and Eq. (4)).

Difference (%)_E =
$$100 \times \frac{ME_i - SE_i}{SE_i}$$
 (3)

Difference
$$(\%)_G = 100 \times \frac{MG_i - SG_i}{SG_i}$$
 (4)

where SE_i and SG_i represent survey EUI for electricity and natural gas of end-use i. ME_i and MG_i refer to modeled EUI for electricity and natural gas of end-use i.

3.3 Building AH calculation

Building AH and its three components were calculated using building prototype's AH intensities, footprint areas, and number of floors (Eq. (5)). First, WRF with a single-layer urban canopy model (WRF-UCM) was used to derive gridded weather conditions with high spatiotemporal resolutions for calculating AH intensities. Hourly air temperature at 2m running at 1 km spatial resolution from WRF-UCM was validated using meteorological station observations with the absolute mean bias of 1.57 °C and the index of agreement of 0.98. Then, the hourly air temperature at 2m data from WRF-UCM was used to update EnergyPlus weather files. Second, AH intensities in three components for each building prototype located in each WRF-UCM grid were calculated using EnergyPlus with calibrated building prototypes and updated weather files.

Specifically, building AH from envelope convection was calculated by adding up "Zone, Average, Surface Outside Face Heat Emission to Air Rate [W]" of all zones in a building prototype. Building AH from zone infiltration and exfiltration was calculated as "HVAC, Sum, Site Total Zone Exfiltration Heat Loss [J]" by adding "HVAC, Sum, Site Total Zone Exhaust Air Heat Loss [J]". Building AH from HVAC system was calculated as "HVAC, Sum, HVAC System Total Heat Rejection Energy [J]" adding "HVAC, Sum, Air System Relief Air Total Heat Loss Energy [J]". Finally, hourly total AH and its three components for each building were calculated.

248
$$AH_{building (i)} = AHI_{t,building (i)}^{WRF-UCM grid (j)} \times A_{building (i)} \times NF_{building (i)}$$
 (5)

where $AHI_{t,building\ (i)}^{WRF-UCM\ grid\ (j)}$ is the hourly building AH intensity of building prototype type t for building i located in WRF-UCM grid j, $A_{building\ (i)}$ is the footprint area of building i, and $NF_{building\ (i)}$ is the number of floors for building i.

4. Result

4.1 Building energy use calibration

After the end-use-based calibration, modeled EUIs of all building prototype agreed well with survey EUIs. Modeled-survey EUIs for all building prototypes ranged from -8.2 to 9.8% for electricity and -10.0 to 7.7% for natural gas (Figure 4A and B), which were up to 110% and 135% without calibration, respectively. In general, the performance of calibration for residential building prototypes was the best, and their modeled-survey EUIs for both electricity and natural gas after calibration were between -0.6% and 3%. Among commercial building prototypes, the performance of calibration for retail, restaurant, and large office building prototypes was the best, and their modeled-survey EUIs for both electricity and natural gas after calibration were between -5% and 5%. In terms of modeled-survey EUIs by end-uses, before calibration, EUIs of equipment and

water heating were more consistent with survey data than those of lighting and HVAC system (Figure 4C). After calibration, modeled-survey EUIs of lighting for commercial prototypes were between 35% to -1.28%, which reached 500% without calibration. For hotel, restaurant, and retail building prototypes, modeled-survey EUI of natural gas HVAC was larger than 200% before calibration and decreased to -15% to 80% after calibration.



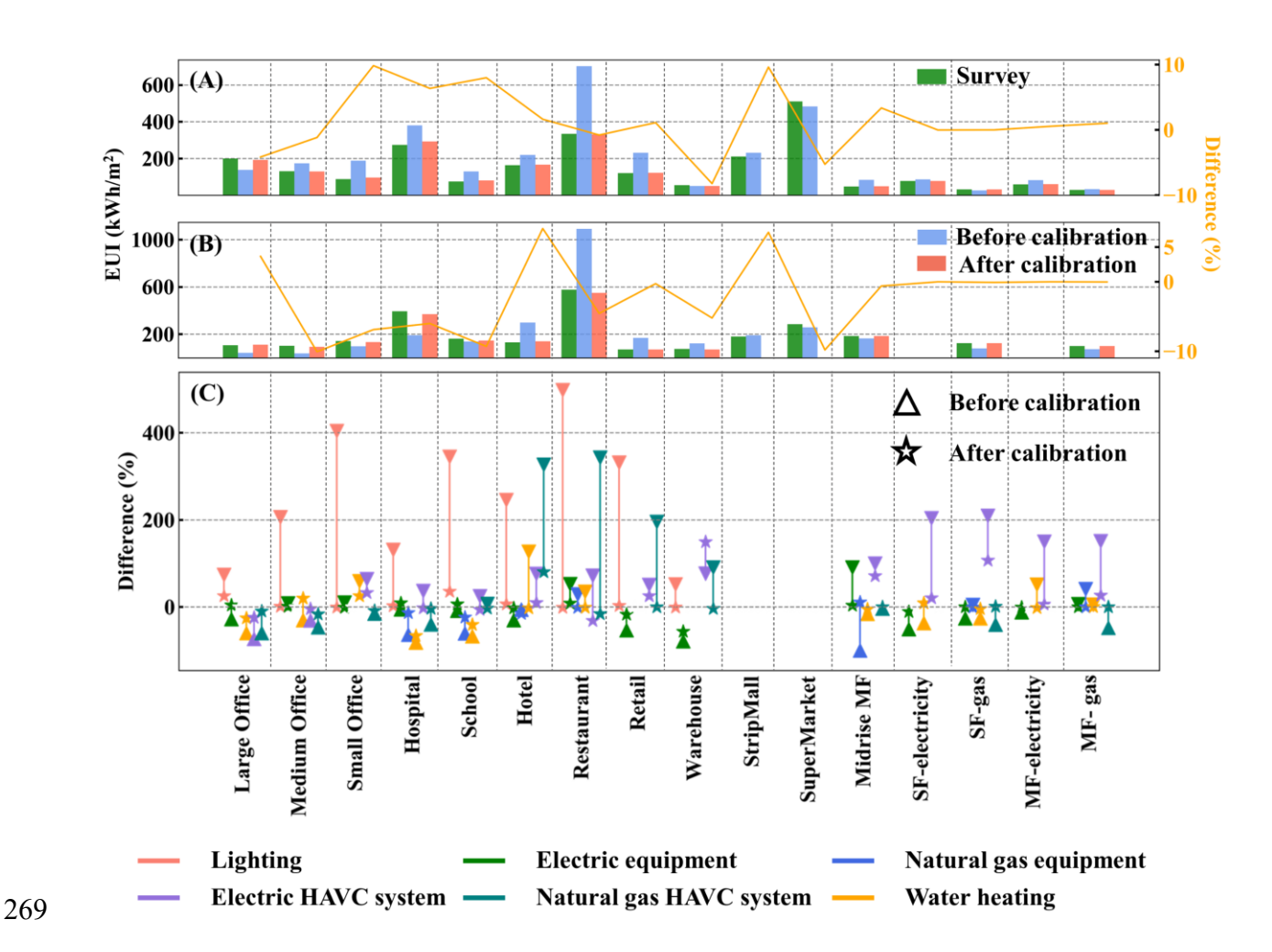


Figure 4. Comparison of calibrated and survey annual electric (A) and natural gas use (B) intensities and the performance of calibration by end-uses (C).

4.2 Annual AH intensity by building types

272

273

274

275

276

277

278

279

280

281

282

283

284

285

286

287

Commercial buildings showed larger intensity (kWh/m²) of annual total AH and larger proportion of AH from HVAC system compared to residential buildings (Figure 5). Two highest annual total AH intensities were restaurant (1393 kWh/m²) and strip mall (1331 kWh/m²). They were about six times large as that of residential buildings of MF-electricity (217 kWh/m²). On average, AH from HVAC system accounted for about 40% of total AH intensity for commercial buildings, while for residential buildings, it only accounted for about 10%. In particular, in buildings with large conditioned areas such as large office and hospital, this component accounted for almost 80% of total AH intensities. However, reversed situation was observed for the other two components. AH from envelope convection and zone infiltration and exfiltration accounted for about 70% and 20% of total AH intensities in residential buildings, respectively, while for commercial buildings except for restaurant, they only accounted for an average of 50% and 10%, respectively. Particularly, large variability of AH intensities from envelope convection was found for commercial buildings, ranging from 15% for large office to 84% for warehouse. In addition, due to air exhausted through fans in kitchens, the highest proportion (40%) and magnitude (561 kWh/m²) of AH intensity from zone infiltration and exfiltration were found for restaurants.

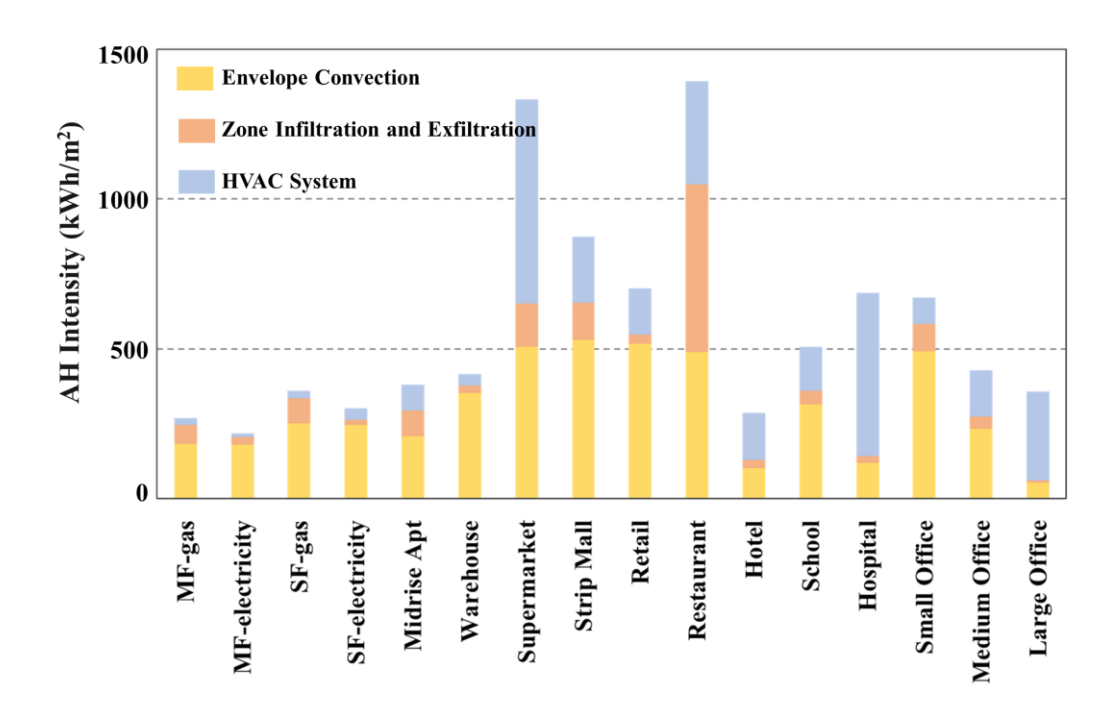


Figure 5. Annual total AH intensity (kWh/m²) and its three components by building types in 2012 in Boston.

4.3 Temporal patterns of building AH

Monthly variations of building AH appeared high in summer and low in winter for total AH and its envelope and HVAC components, while for zone component, the monthly pattern was reversed (Figure 6). The highest total building AH of commercial (1.36 ×10⁹ kWh) and residential (1.02 ×10⁹ kWh) buildings occurred in July. The lowest total AH occurred in December (0.65 × 10⁹ kWh) for commercial buildings and in October (0.6 ×10⁹ kWh) for residential buildings. Monthly pattern of building AH from envelope convection was consistent with the seasonal change of solar radiation, reaching the highest value (1.58 ×10⁹ kWh) in July and lowest value (0.32 ×10⁹ kWh) in December. Building AH from zone infiltration and exfiltration reached the highest value

 $(0.56 \times 10^9 \text{ kWh})$ in January and lowest value $(0.05 \times 10^9 \text{ kWh})$ in August due to small difference in enthalpies between exhaust and outdoor air in summer (Hong et al., 2020). Unlike the other two components, building AH from HVAC system showed two peaks around July and January. The first peak $(0.8 \times 10^9 \text{ kWh})$ appeared in summer because of its high heat emissions from relief air for cooling use, whereas the winter maximum $(0.65 \times 10^9 \text{ kWh})$ was due to its high reject heat emissions from combustion exhaust for heating use.

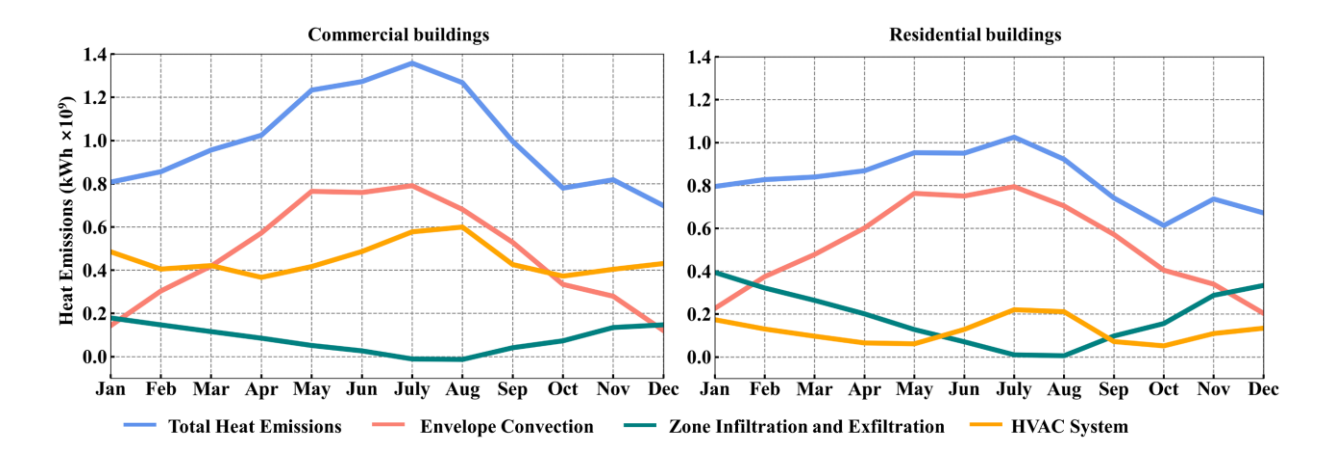


Figure 6. Monthly total building AH and its three components of commercial and residential buildings in Boston in 2012.

Except for zone component, hourly total building AH and its envelope and HVAC components exhibited significant variations with the highest AH in afternoon and the lowest AH at midnight (Figure 7). Diurnal variations of AH from envelope convection followed diurnal changes of solar radiation. In summer, AH from envelope convection increased dramatically between 5 am to 8 pm and reached its peak (7.0 ×10⁶ kWh) at noon. In winter, it increased dramatically between 7 am to 6 pm and reached its peak (5.7 ×10⁶ kWh) at 1 pm. The trend of

building AH from HVAC system was strongly affected by operation schedules of occupants and outdoor air temperature. When HVAC system was on between 6 am to 10 pm, the trend of AH from HVAC system was related to outdoor air temperature in summer, reaching its peak (3.0 ×10⁶ kWh) at 4 pm. The peak period in residential buildings (between 2 pm to 6 pm) occurred 1 hour later than that in commercial buildings (between 1pm to 5 pm). However, diurnal variations of this component in winter were not significant, especially in residential buildings. AH from zone infiltration and exfiltration showed small fluctuation around 1.4 ×10⁶ kWh in winter and large fluctuation in the daytime of summer with the lowest value (-0.6×10⁶ kWh) at 2 pm.

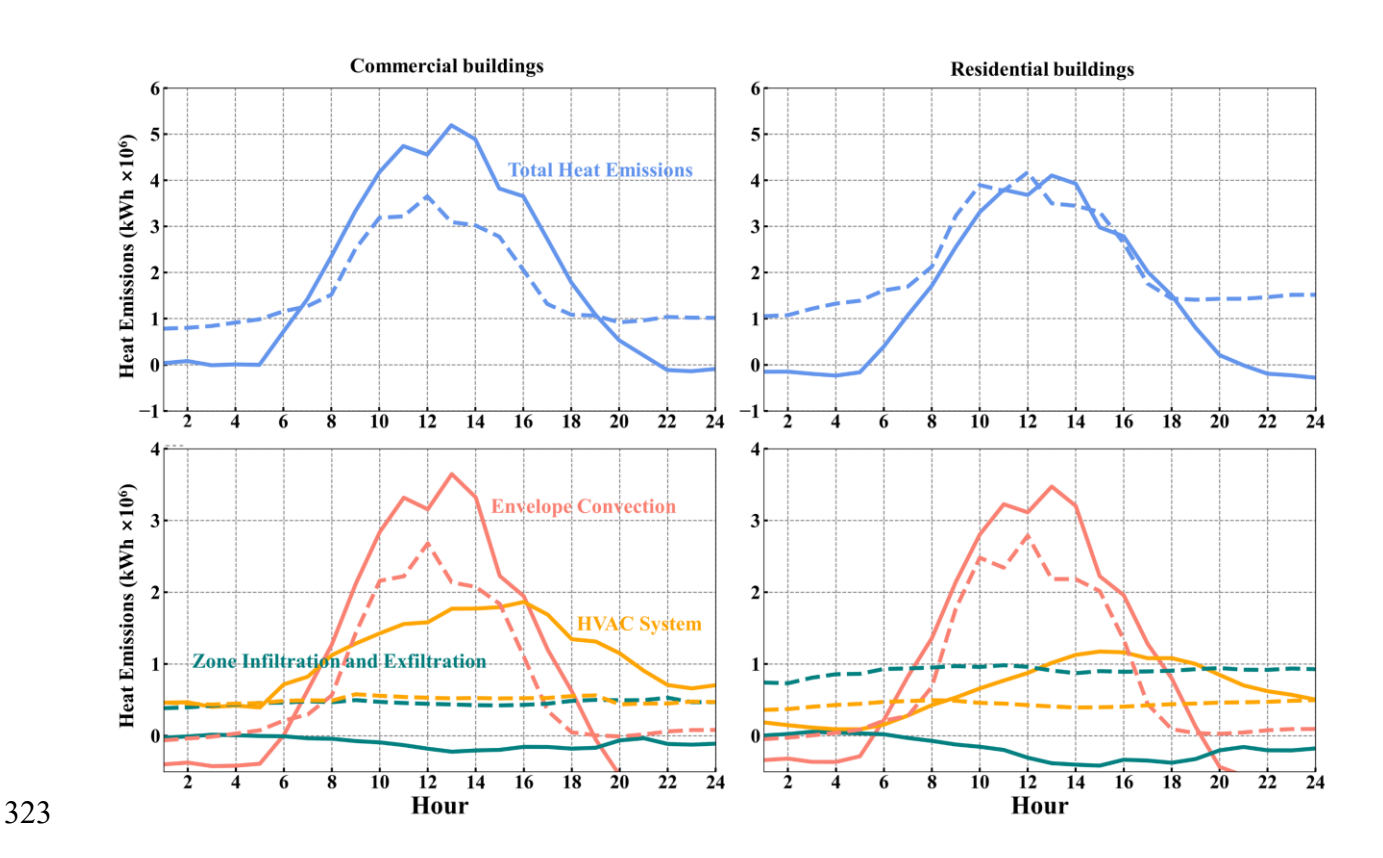


Figure 7. Hourly building AH and its three components of commercial and residential buildings on the coldest day (January 15, marked with dash line) and hottest day (July 17, marked with solid line) in 2012 in Boston.

4.4 Spatial patterns of building AH

At the individual building level, the annual total building AH reached 9.7×10⁸ kWh in downtown, while it was down to 35 kWh in suburb (Figure 8A). Building AH from HVAC system showed the largest downtown-suburban gradient (Figure 8D), falling from 8.1×10⁸ kWh in downtown to 4.7 kWh in suburb. Building AH from zone infiltration and exfiltration exhibited the smallest downtown-suburban gradient (Figure 8C), dropping from 1.0×10⁸ kWh in downtown to 4.7 kWh in suburb. Buildings with annual total AH larger than 10.4×10⁵ kWh were mainly distributed in downtown crowded with tall and commercial buildings (e.g., offices, hotels, and hospitals). Buildings with annual total AH less than 1.0×10⁵ kWh were found in suburb covered by single- and multi-family houses.

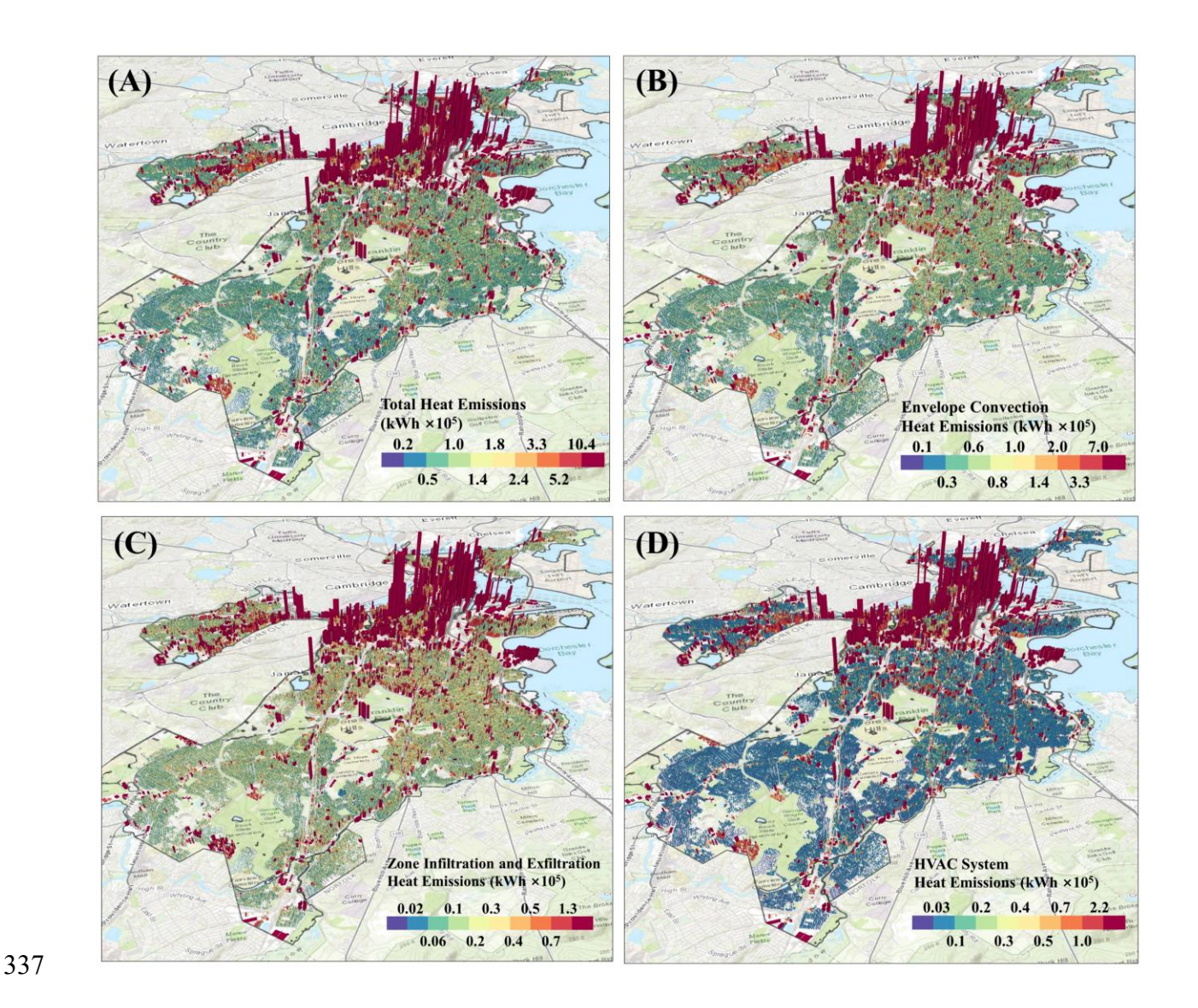


Figure 8. Spatial patterns of the total annual building AH (A) and AH from envelope convection (B), zone infiltration and exfiltration (C), and HVAC system (D) in Boston in 2012.

Densities (kWh/m²) of total building AH were highest in Back Bay neighborhood and lowest in East Boston neighborhood (Figure 9). Density of building AH here was the ratio of the sum of building AH in a neighborhood and the area of neighborhood. In summer, the density of total AH of Back Bay neighborhood reached the maximum value of 526 kWh/m², of which 56% was from HVAC system and 44% was from envelope convection. In winter, total AH density of Back Bay neighborhood reached the minimum value of 369 kWh/m², of which 54% was from HVAC system,

346 followed by envelope convection (24%) and zone infiltration and exfiltration (22%). Southern and 347 northern suburban neighborhoods (i.e., West Roxbury, Roslindale, Hyde Park, Mattapan, and East Boston) showed a lower density of total AH than 30 kWh/m² in summer and 20 kWh/m² in winter. 348 349 For most of neighborhoods, seasonal variations of total building AH were not as dramatic as 350 its three components because of changes in the proportion of these three components among total 351 AH in different seasons. In spring, summer, and fall, except for urban core neighborhoods such as 352 Back Bay, West End, and Longwood, building AH from envelope convection was the most 353 dominant component with a proportion over 65%, determining spatial patterns of total building 354 AH in these three seasons. This component did not show significant difference between spring and 355 summer because of its monthly high AH in May, June, and July (end of spring and start of summer). 356 In winter, the proportion of three AH components among total AH was similar, jointly determining

357

spatial patterns of total AH.

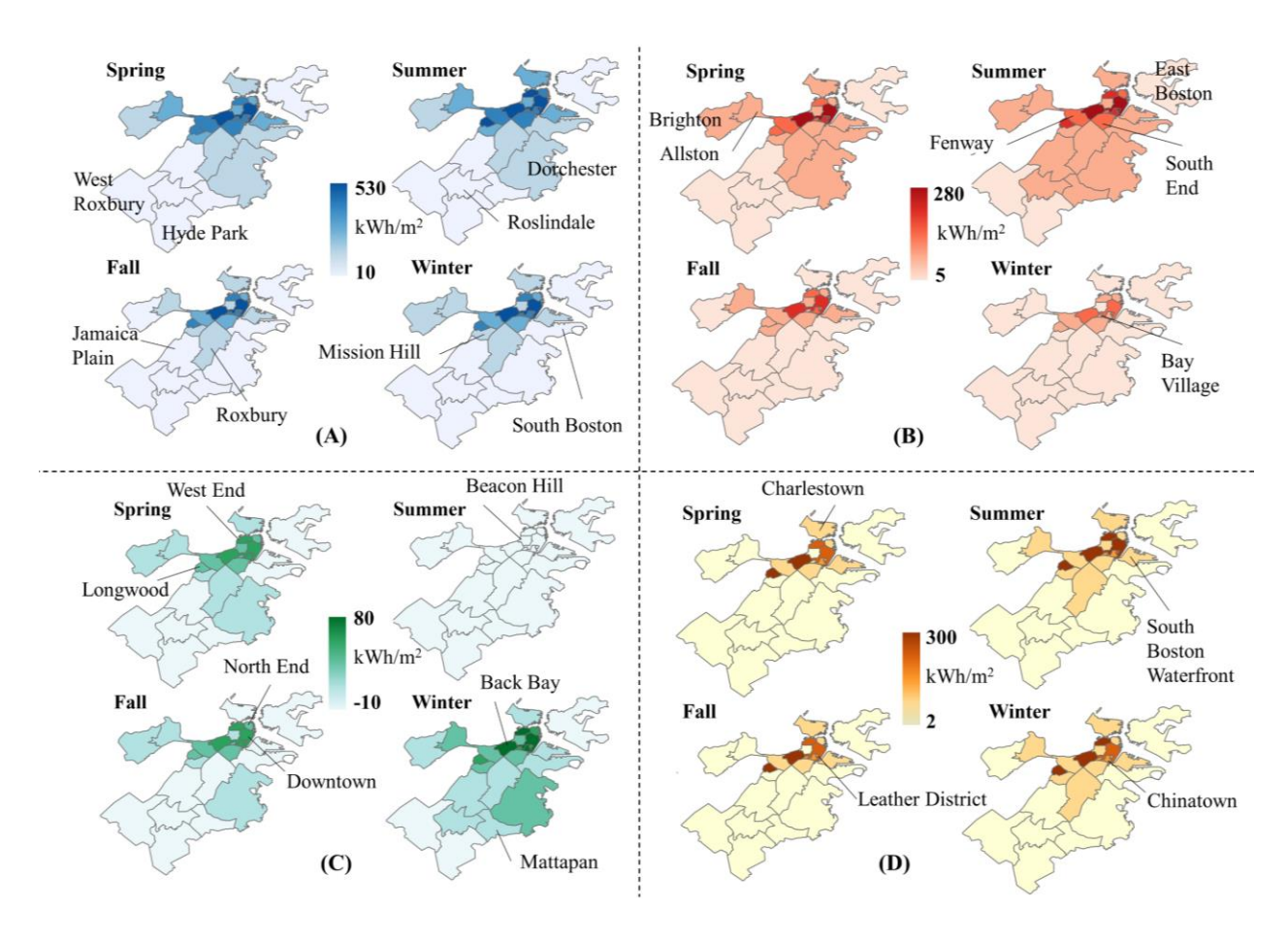


Figure 9. Densities (kWh/m²) of seasonal total building AH (A) and AH from envelope convection (B), zone infiltration and exfiltration (C), and HVAC system (D) at the neighborhood level in Boston in 2012.

5. Discussion

The magnitude of building AH and its component varied among building types due to a variability of geometry structures, HVAC systems, and construction materials of buildings. For instance, small office and warehouse prototypes are characterized by a small building area with a relatively large surface-to-volume ratio (Hong et al., 2020), causing a large share of AH from envelope component. Since central cooling systems with a chilled water plant are always needed for large buildings to meet intensive cooling loads (Hong et al., 2020), large office and hospital

buildings equipped with cooling towers demonstrated a large share of AH from HVAC component. Thermal resistance of construction materials in residential buildings was lower than that in commercial building prototypes, resulting in relatively larger share of AH from envelope component.

The knowledge about spatiotemporal patterns of building AH from this study has a potential to assist policymakers in developing building energy-saving strategies tailored to a specific city or region, which in turn facilitates smart city planning and sustainable urban development. For example, West Roxbury, Hyde Park, Roslindale, and East Boston neighborhoods show the largest share (up to 65%) of heat emissions from envelope conduction, informing local governments to prioritize reducing building AH from envelope conduction in northern and southern suburban areas. Additional high-resistivity insulation layer on the exterior surfaces of buildings can be considered to limit conductive heat flow (Ferrando et al., 2021). Longwood, Back Bay and West End neighborhoods show the largest share (up to 55%) of heat emissions from the HVAC system. Actions related to the efficiency improvement of HVAC system can be prioritized to reduce total AH in these neighborhoods.

The dataset of hourly building AH at individual building level can be aggregated into very high spatial resolution, for numerical weather prediction models (e.g., Weather Research and Forecasting (WRF) Model) to quantify the magnitude of its contribution to UHI and explore the effects of different urban heat mitigation strategies. Driven by building AH data, numerical weather prediction models can better represent the spatial heterogeneity of building AH, and therefore help to investigate how building AH can influence urban thermal environment at high spatial resolution. Moreover, driven by building AH data under different scenarios of building efficiency improvement, numerical weather prediction models can be used to explore the role of

building AH in mitigating UHI effect, providing scientific basis for developing urban heat mitigation and adaption measures in Boston.

Our calibration method of the city-scale building energy use modeling can provide a feasible solution to accurately calibrate building energy consumption in other areas by capitalizing on an advantage of nationwide coverage of two datasets, i.e., building energy surveys and building prototypes. CBECS and RECS are the largest building energy surveys to date conducted by the EIA(Deng et al., 2018), reporting over 12,000 residential and 6,700 commercial buildings' annual energy consumption in the U.S., disaggregating by energy sources and end-uses. PNNL and DOE developed building prototypes across 16 locations representing all U.S. climate zones. However, the proposed method is restrained to using survey data with end-use information. It is challenging to conduct monthly calibration using the proposed method because monthly metered utility data are usually not specified for end-use categories. When utility meter data become widely available, monthly or hourly calibration can be developed to improve building energy use and AH modeling.

This study opened future research avenues. For example, large scale building type (e.g., office, restaurant, hospital, school, retail, hotel, and residence) mapping methods are highly needed to support building AH estimation, especially in areas with limited data availability. Together with the support of existing large scale building footprint ("Microsoft US Building Footprints," 2018) and height (Li et al., 2020) datasets, the city-scale building AH models can be used to investigate historical and future urban building AH under different climate and policy scenarios, offering supports for government policy making and city sustainable development planning.

6. Conclusions

In this study, a framework named CityBHEM was developed to estimate building AH and its three components at single building level and hourly scale and implemented this framework in

the study area of Boston. First, sixteen building prototypes were selected based on building type, construction year, and foundation type in Boston. Second, an end-use-based calibration of building energy use for each prototype was developed to ensure the performance of EnergyPlus calculation. Finally, hourly building AH and its three components for each building in Boston were estimated using AH intensities from calibrated prototypes together with building types and sizes.

Our results from the CityBHEM revealed spatiotemporal patterns of building AH and its three components in Boston. Spatially, the annual total building AH reached 9.7×10⁸ kWh in downtown, while it was only 35 kWh in suburb. AH from HVAC system is a main contributor of large downtown-suburban gradient, followed by envelope convection and zone infiltration and exfiltration. Temporally, AH from envelope convection and HVAC system in July were significantly higher than those in January, with a diurnal peak at noon and 4pm, respectively. AH from zone infiltration and exfiltration in January was significantly higher than that in July, with small diurnal fluctuations.

The proposed CityBHEM by integrating publicly available datasets and physical modeling is transferable to other U.S. cities, offering great support for UHI studies and city sustainable development planning. The resulting datasets can serve as a reliable input for numerical weather predication models in UHI studies to improve the understanding of feedbacks between urban systems and the atmosphere. The improved understanding of building AH from various components is of great help for policymakers in developing building energy-saving strategies tailored to a specific region within cities. To improve monthly or hourly patterns of building energy use and AH modeling performance, metered utility data will be of help for developing monthly or hourly calibration method in future studies. Another possible future research avenue is the

- development of large scale building type mapping methods to support building AH estimation with
- 438 high spatiotemporal details in areas with limited data availability.

439

440 CRediT authorship contribution statement

- 441 Wei Chen: Methodology, Software, Validation, Investigation, Writing Original Draft. Yuyu
- **Zhou:** Conceptualization, Methodology, Writing review & editing, Supervision, Funding
- acquisition. Yanhua Xie: Writing review & editing. Gang Chen: Writing review & editing.
- 444 **Ke Jack Ding:** Writing review & editing. **Dan Li:** Writing review & editing.

445 Acknowledgement

- This work was supported by the National Science Foundation (No.1854502). We would like to
- thank two anonymous reviewers for their constructive comments and suggestions.

448 References

- 449 ASHRAE Standards 55, 2017. Thermal Environmental conditions for human occupancy.
- 450 ASHRAE Standards 90.1, 1999. Energy Standard for Buildings Except for Low-Rise Residential
- 451 Buildings.
- 452 ASHRAE Standards 90.2, 2007. Energy Efficient Design of Low-Rise Residential Buildings.
- 453 Chang, Y., Xiao, J., Li, Xuxiang, Frolking, S., Zhou, D., Schneider, A., Weng, Q., Yu, P., Wang,
- 454 X., Li, Xing, 2021. Exploring diurnal cycles of surface urban heat island intensity in Boston
- with land surface temperature data derived from GOES-R geostationary satellites. Sci. Total
- 456 Environ. 763, 144224.
- 457 Chen, S., Hu, D., Wong, M.S., Ren, H., Cao, S., Yu, C., Ho, H.C., 2019. Characterizing
- spatiotemporal dynamics of anthropogenic heat fluxes: A 20-year case study in Beijing-
- Tianjin–Hebei region in China. Environ. Pollut. 249, 923–931.
- 460 Chen, Y., Deng, Z., Hong, T., 2020. Automatic and rapid calibration of urban building energy
- 461 models by learning from energy performance database. Appl. Energy 277, 115584.
- Chow, W.T.L., Salamanca, F., Georgescu, M., Mahalov, A., Milne, J.M., Ruddell, B.L., 2014. A
- multi-method and multi-scale approach for estimating city-wide anthropogenic heat fluxes.
- 464 Atmos. Environ. 99, 64–76.
- 465 Chrysoulakis, N., Grimmond, C.S.B., 2016. Understanding and reducing the anthropogenic heat
- emission. Urban Clim. Mitig. Tech. Santamouris, M., Kolokotsa, D., Eds 27–40.
- 467 Crawley, D.B., Lawrie, L.K., Winkelmann, F.C., Buhl, W.F., Huang, Y.J., Pedersen, C.O.,
- Strand, R.K., Liesen, R.J., Fisher, D.E., Witte, M.J., 2001. EnergyPlus: creating a new-
- generation building energy simulation program. Energy Build. 33, 319–331.

- 470 Deng, H., Fannon, D., Eckelman, M.J., 2018. Predictive modeling for US commercial building
- 471 energy use: A comparison of existing statistical and machine learning algorithms using
- 472 CBECS microdata. Energy Build. 163, 34–43.
- Dhakal, S., Hanaki, K., Hiramatsu, A., 2004. Heat discharges from an office building in Tokyo
- 474 using DOE-2. Energy Convers. Manag. 45, 1107–1118.
- Dhakal, S., Hanaki, K., Hiramatsu, A., 2003. Estimation of heat discharges by residential
- buildings in Tokyo. Energy Convers. Manag. 44, 1487–1499.
- 477 DOE, U.S., 2015. An assessment of energy technologies and research opportunities. Quadrenn.
- 478 Technol. Rev. United States Dep. Energy.
- 479 Dong, Y., Varquez, A.C.G., Kanda, M., 2017. Global anthropogenic heat flux database with high
- spatial resolution. Atmos. Environ. 150, 276–294.
- Ferrando, M., Hong, T., Causone, F., 2021. A simulation-based assessment of technologies to
- reduce heat emissions from buildings. Build. Environ. 195, 107772.
- Hong, T., Ferrando, M., Luo, X., Causone, F., 2020. Modeling and analysis of heat emissions
- from buildings to ambient air. Appl. Energy 277, 115566.
- Hong, T., Yang, J., Luo, X., 2019. Heat Emissions from Buildings to Ambient Air. BS2019,
- 486 Rome, Italy Proc.
- 487 Hsieh, C.-M., Aramaki, T., Hanaki, K., 2007. Estimation of heat rejection based on the air
- 488 conditioner use time and its mitigation from buildings in Taipei City. Build. Environ. 42,
- 489 3125–3137.
- 490 Li, W., Zhou, Y., Cetin, K.S., Yu, S., Wang, Y., Liang, B., 2018. Developing a landscape of
- 491 urban building energy use with improved spatiotemporal representations in a cool-humid

- 492 climate. Build. Environ. 136, 107–117.
- Li, X., Zhou, Y., Gong, P., Seto, K.C., Clinton, N., 2020. Developing a method to estimate
- building height from Sentinel-1 data. Remote Sens. Environ. 240, 111705.
- Li, Xiaoma, Zhou, Y., Asrar, G.R., Imhoff, M., Li, Xuecao, 2017. The surface urban heat island
- response to urban expansion: A panel analysis for the conterminous United States. Sci.
- 497 Total Environ. 605–606, 426–435. https://doi.org/10.1016/j.scitotenv.2017.06.229
- Lindberg, F., Grimmond, C.S.B., Yogeswaran, N., Kotthaus, S., Allen, L., 2013. Impact of city
- changes and weather on anthropogenic heat flux in Europe 1995–2015. Urban Clim. 4, 1–
- 500 15.
- Liu, X., Yue, W., Zhou, Y., Liu, Y., Xiong, C., Li, Q., 2021. Estimating multi-temporal
- anthropogenic heat flux based on the top-down method and temporal downscaling methods
- in Beijing, China. Resour. Conserv. Recycl. 172, 105682.
- Lu, Y., Wang, Q., Zhang, Y., Sun, P., Qian, Y., 2016. An estimate of anthropogenic heat
- emissions in China. Int. J. Climatol. 36, 1134–1142.
- 506 Luo, X., Vahmani, P., Hong, T., Jones, A., 2020. City-Scale Building Anthropogenic Heating
- during Heat Waves. Atmosphere (Basel). 11, 1206.
- Masson, V., 2000. A physically-based scheme for the urban energy budget in atmospheric
- models. Boundary-layer Meteorol. 94, 357–397.
- Melaas, E.K., Wang, J.A., Miller, D.L., Friedl, M.A., 2016. Interactions between urban
- vegetation and surface urban heat islands: a case study in the Boston metropolitan region.
- 512 Environ. Res. Lett. 11, 54020.
- 513 Microsoft US Building Footprints [WWW Document], 2018. URL

- 514 https://github.com/Microsoft/USBuildingFootprints
- Nie, W.-S., Sun, T., Ni, G.-H., 2014. Spatiotemporal characteristics of anthropogenic heat in an
- urban environment: A case study of Tsinghua Campus. Build. Environ. 82, 675–686.
- O'Neill, Z., Eisenhower, B., Yuan, S., Bailey, T., Narayanan, S., Fonoberov, V., 2011. Modeling
- and calibration of energy models for a DoD building. ASHRAE Trans. 117, 358.
- 519 Qiu, S., Li, Zhengwei, Pang, Z., Zhang, W., Li, Zhenhai, 2018. A quick auto-calibration
- approach based on normative energy models. Energy Build. 172, 35–46.
- Sailor, D.J., 2011. A review of methods for estimating anthropogenic heat and moisture
- emissions in the urban environment. Int. J. Climatol. 31, 189–199.
- Sailor, D.J., Brooks, A., Hart, M., Heiple, S., 2007. A bottom-up approach for estimating latent
- and sensible heat emissions from anthropogenic sources, in: Seventh Symposium on the
- 525 Urban Environment, San Diego, California. pp. 10–13.
- Sailor, D.J., Georgescu, M., Milne, J.M., Hart, M.A., 2015. Development of a national
- anthropogenic heating database with an extrapolation for international cities. Atmos.
- 528 Environ. 118, 7–18.
- Sailor, D.J., Lu, L., 2004. A top-down methodology for developing diurnal and seasonal
- anthropogenic heating profiles for urban areas. Atmos. Environ. 38, 2737–2748.
- Santos, L.G.R., Singh, V.K., Mughal, M.O., Nevat, I., Norford, L.K., Fonseca, J.A., 2020.
- Estimating building's anthropogenic heat: a joint local climate zone and land use
- classification method, in: ESIM Conference 2021.
- Sun, K., Hong, T., Taylor-Lange, S.C., Piette, M.A., 2016. A pattern-based automated approach
- to building energy model calibration. Appl. Energy 165, 214–224.

537 K., Kaneyasu, N., 2017. A climatological validation of urban air temperature and electricity 538 demand simulated by a regional climate model coupled with an urban canopy model and a 539 building energy model in an Asian megacity. Int. J. Climatol. 37, 1035–1052. 540 Wang, J.A., Hutyra, L.R., Li, D., Friedl, M.A., 2017. Gradients of atmospheric temperature and 541 humidity controlled by local urban land-use intensity in Boston, J. Appl. Meteorol. 542 Climatol. 56, 817–831. 543 Xie, M., Liao, J., Wang, T., Zhu, K., Zhuang, B., Han, Y., Li, M., Li, S., 2016. Modeling of the 544 anthropogenic heat flux and its effect on regional meteorology and air quality over the 545 Yangtze River Delta region, China. Atmos. Chem. Phys. 16, 6071–6089. 546 Yu, M., Carmichael, G.R., Zhu, T., Cheng, Y., 2014. Sensitivity of predicted pollutant levels to 547 anthropogenic heat emissions in Beijing. Atmos. Environ. 89, 169–178. 548 Zhou, Y., Li, X., Asrar, G.R., Smith, S.J., Imhoff, M., 2018. A global record of annual urban 549 dynamics (1992–2013) from nighttime lights. Remote Sens. Environ. 219, 206–220. 550 Zhou, Y., Smith, S.J., Elvidge, C.D., Zhao, K., Thomson, A., Imhoff, M., 2014. A cluster-based 551 method to map urban area from DMSP/OLS nightlights. Remote Sens. Environ. 147, 173– 552 185. 553 Zhou, Y., Weng, Q., Gurney, K.R., Shuai, Y., Hu, X., 2012. Estimation of the relationship 554 between remotely sensed anthropogenic heat discharge and building energy use. ISPRS J. 555 Photogramm. Remote Sens. 67, 65–72.

Takane, Y., Kikegawa, Y., Hara, M., Ihara, T., Ohashi, Y., Adachi, S.A., Kondo, H., Yamaguchi,

536

556